

Indoor MIMO Measurements at 2.55 and 5.25 GHz – a Comparison of Temporal and Angular Characteristics

Ernst Bonek¹, Nicolai Czink¹, Veli-Matti Holappa², Mikko Alatossava²,
Lassi Hentilä³, Jukka-Pekka Nuutinen³, Arindam Pal⁴

¹Institut für Nachrichtentechnik und Hochfrequenztechnik, Technische Universität Wien, Vienna, Austria

²Centre for Wireless Communications, Oulu University, Oulu, Finland

³Elektrobit Testing Ltd., Oulu, Finland

⁴University of Bristol, Bristol, UK

E-Mail: ernst.bonek@tuwien.ac.at

Abstract—Indoor MIMO measurements in a laboratory environment, covering both line-of-sight (LoS) and obstructed line-of-sight (OLoS), are reported. Comparison of data taken at 2.55 and 5.25 GHz reveal subtle differences in temporal and angular characteristics. Multipath appears in clusters, which can be attributed to specific scattering/reflection areas in the environment.

I. INTRODUCTION

Whereas the body of MIMO measurements in various frequency bands is increasing, see e.g. the upcoming summary of the large body of such measurements in COST 273 [1], comparisons of measurements at different frequencies in one and the same environment are scarce [2]. Such comparisons will assist the transfer of modelling approaches from one frequency range to another, while catching the essential temporal and spatial features. Likeness found will make MIMO channel models more robust, differences will highlight the necessary changes when extrapolating to another frequency band. Ray-tracing tools can be calibrated better by measurements at different frequencies. For instance, what role does the surface roughness of walls and the reflection/scattering properties of furniture and laboratory equipment play?

Advanced MIMO channel modelling must include the directional component of the channel. It has turned out convenient to account for this directional component by grouping the multipath components (MPCs) to *clusters* [3]. A cluster is a group of MPCs showing similar angles of arrival and departure (AoAs, AoDs), delays, and/or Doppler frequencies. As the term “similar” is vague, clustering is a much-discussed topic. The identification of paths with the real environment is strongly aided by measurements at two different frequencies in the very same environment. If clusters identified at one frequency show up at twice the frequency as well and can thus be reliably related to scattering objects and areas, this would constitute strong support for the usefulness of the cluster concept in general. If so, does the similarity bear out both in LoS and NLoS situations? Is there a significant difference in scattering objects?

By comparing double-directional high-resolution MIMO measurements in an indoor environment this paper will focus

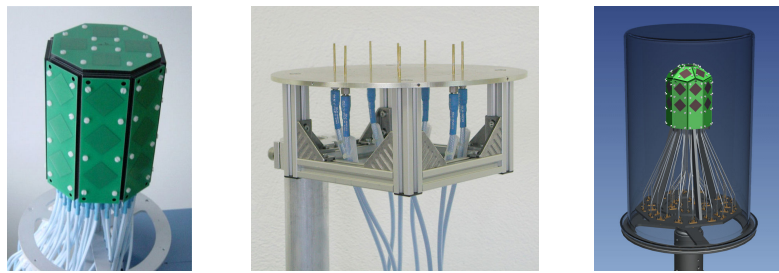
TABLE I
SOUNDER PARAMETERS

Parameter	2.55 GHz	5.25 GHz
Transmit power [dBm]	26	26
Bandwidth [MHz]	200	200
Chip frequency [MHz]	100	100
Number of TX antennas	56	50
Number of RX antennas	8	32
Code length [μ s]	2.55	2.55
Channel sampling rate [Hz]	92.6	59.4
Cycle duration [μ s]	1542.24	8415.00
TX antenna height [m]	1.53	1.53
RX antenna height [m]	1.05	0.82

on differences/similarities of delay characteristics and the angular distribution of incoming/outgoing waves in azimuth. Polarization and elevation would be also interesting, but are not investigated here.

II. MEASUREMENT EQUIPMENT AND SET-UP

In this study we applied a wideband radio channel sounder, Propsound CS, which utilizes periodic pseudo-random binary signals. The sounder is described in more detail in [4]. In sounding, M-sequences with adjustable code lengths are employed and sent using a time-division multiplexed switching of transmit and receive antennas. The spread spectrum signal has 100 Mchip/s chip rate and switches through all the antennas with the cycle rates presented in Table I. Thus, sequential radio channel measurement between all possible TX and RX antenna pairs is achieved by antenna switching at both the transmitter and the receiver. The number of antenna elements used is proportional to the cycle rate. The sounder was operated in burst-mode, i.e. after four measuring cycles there was a break to allow real-time data transfer to the control laptop computer. During the measurements, a real-time display of the received impulse responses (IRs) can be monitored from the control laptop computer. In addition to basic data handling features, the post-processing tools include the ISISTM (Initialization and Search Improved SAGE) software, which is based on a super-resolution SAGE algorithm employing maximum likelihood techniques for parameter estimation [5].



(a) 3x8 ODA, 2.55 GHz (b) 7+1 UCA, 2.55 GHz (c) 2x9 ODA, 5.25 GHz

Fig. 1. Antenna arrays. (a) 2.55 GHz omni-directional patch array (ODA), (b) 2.55 GHz circular monopole array (UCA), (c) 5.25 GHz ODA.

TABLE II
ANTENNA PARAMETERS

Antenna	Azimuth coverage	Elevation coverage
3x8 ODA 2.55 GHz	$-180^\circ \dots 180^\circ$	$-55^\circ \dots 90^\circ$
7+1 UCA 2.55 GHz	$-180^\circ \dots 180^\circ$	$0^\circ \dots 60^\circ$
2x9 ODA 5.25 GHz	$-180^\circ \dots 180^\circ$	$-55^\circ \dots 90^\circ$

The selected antenna arrays illustrated in Figure 1 are able to capture largely the spatial characteristics of the radio channel at *both* link-ends. The 2.55 GHz array (Figure 1a) used at the TX consists of 28 dual-polarized patch elements. The elements are positioned in a way that allows channel probing in the *full* azimuth domain and almost full coverage of the elevation. Only a small cone in space angle along the supporting pole of the array cannot be covered. Figure 1b shows the uniform circular array with 7+1 monopoles used at the RX end at 2.55 GHz. It supports full azimuth direction probing but not the elevation. At 5.25 GHz both TX and RX had 25 element patch arrays shown in Figure 1c. Their properties are similar to the 2.55 GHz patch array. Table II shows the azimuth and elevation coverage of the antennas. All antennas had been calibrated in an anechoic chamber. The signal model on which SAGE is based is using the array pattern data over rotation of the array as a base to calculate the response of each element to waves impinging from different angles. In the calibration process, the antenna pattern of each single element was measured in amplitude and phase over azimuth and elevation, resulting in an azimuth / elevation matrix. This measurement was done for both horizontal and vertical polarization. To minimize the interference of WLAN and Bluetooth, the center frequency for the measurements was chosen to be 2.55 GHz. Still, there seems to have been (spurious) radiation from these devices above 2.45 GHz, so we had to expect an enhanced noise floor in the IRs. The ensuing smaller dynamic range resulted in a smaller number of paths ISIS could extract from the measurement.

III. SCENARIOS

We took numerous measurements, of which we analyse a particularly interesting one in this paper. It is a medium-sized laboratory room with dimensions of 10 m \times 11 m (Figure 2). To facilitate comparison of results, exactly the same routes were measured on successive measurements with different

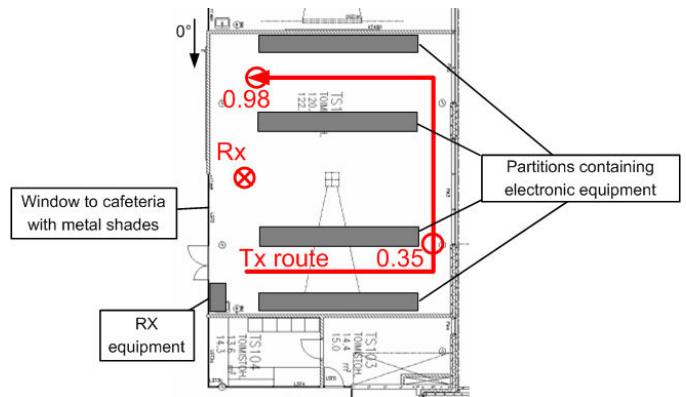


Fig. 2. Measurement route in the medium-sized laboratory. The antenna orientation of 0° is the same for both Tx and Rx antennas.

channel sounder radio modules for the two above mentioned carrier frequencies.

The measurement route changed from LoS to OLoS (direct line of sight obstructed by partitions, equipped with laboratory instruments), back to LoS, then OLoS again and finished with LoS. Figure 3 shows the situation around the transmitter and the receiver, respectively.

IV. DELAY RESULTS

We calculated received power by integration over the averaged IR (averaged over 448/1600 actually recorded IRs between all possible antenna pairs at 2.55/5.25GHz) up to 1 microsecond¹.

Figure 4 compares received power at the two frequencies. It seems as if the temporal response at 5.25 GHz would show greater detail in the long-delayed tail of the IR. This result, observed in other environments as well, is insofar interesting as the temporal resolution of the measuring instruments was the same at both frequencies.

There are conflicting changes of the scattering/reflection properties of the environment imaginable when going to higher frequency. First, as the ratio of random surface irregularities to wavelength gets larger, specular reflections gradually change to true scattering in every direction. Hence, more unresolvable multipath will occur, and impulse responses should exhibit

¹Integration over five microseconds including the noise level or subtracting it prior to integration gave results that deviated less than 0.5 dB

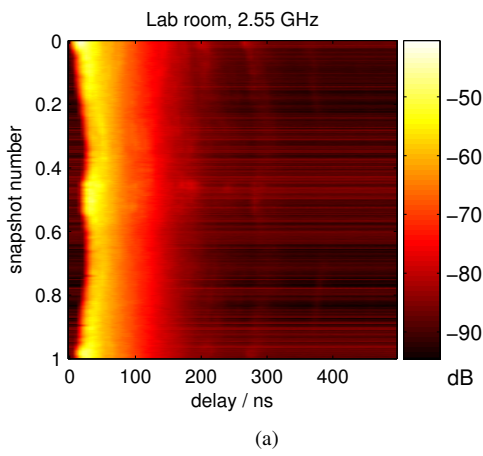


(a)

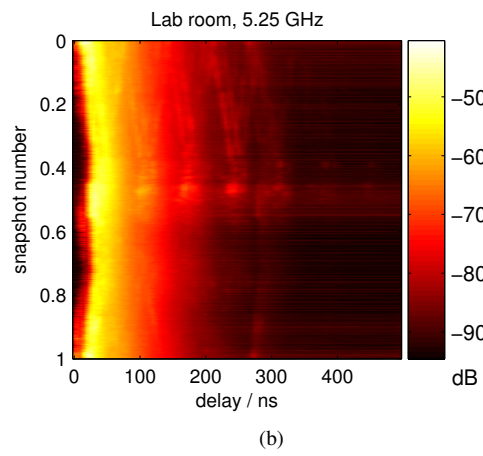


(b)

Fig. 3. Photographs of the environment with (a) Rx opposite the window, (b) Tx at the starting point of the route.

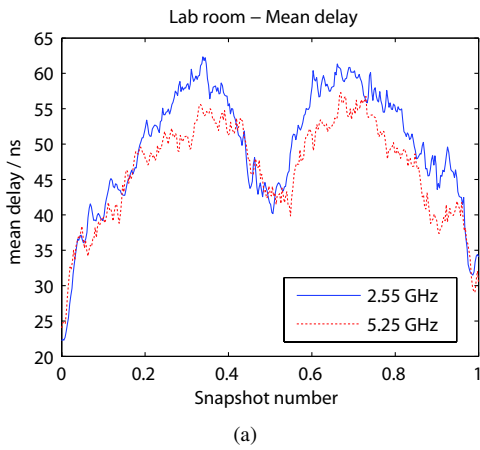


(a)

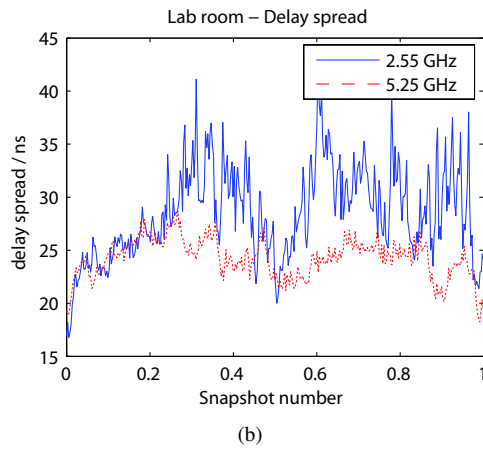


(b)

Fig. 4. Received power vs. delay and snapshot number in the considered environment. a) 2.55 GHz; b) 5.25 GHz.



(a)



(b)

Fig. 5. Mean delay (a) and delay spread (b) vs. normalized snapshot number in the considered environment. Blue solid: 2.55 GHz; red dashed: 5.25 GHz.

more of Richter's "dense multipath" decay [6]. On the other hand, higher frequencies will reveal smaller structures as significant interaction points for electromagnetic waves. Smaller wavelength also means narrower Fresnel ellipsoids, i.e. smaller

"smooth" surfaces will suffice to constitute a mirror, resulting in more specular reflections. Our results support the second explanation more. Figure 5 shows the mean delay and delay spread vs. the normalized snapshot number in the considered

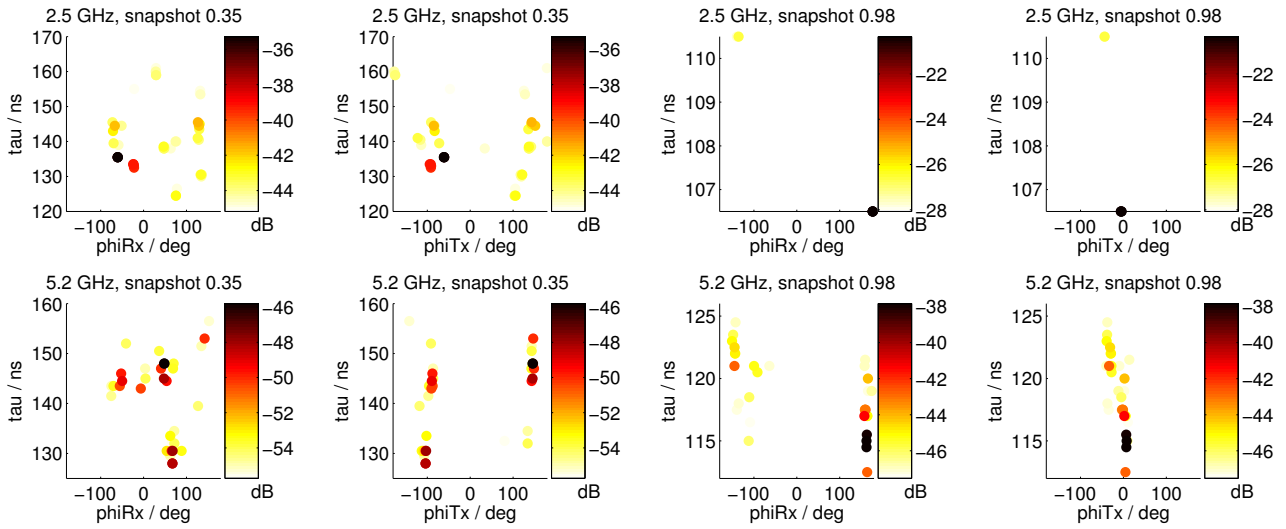


Fig. 6. Outgoing/incoming paths in OLoS (labelled 0.35) and LoS (labelled 0.98) situations (see Figure 2 for location of normalised snapshots and antenna orientations).

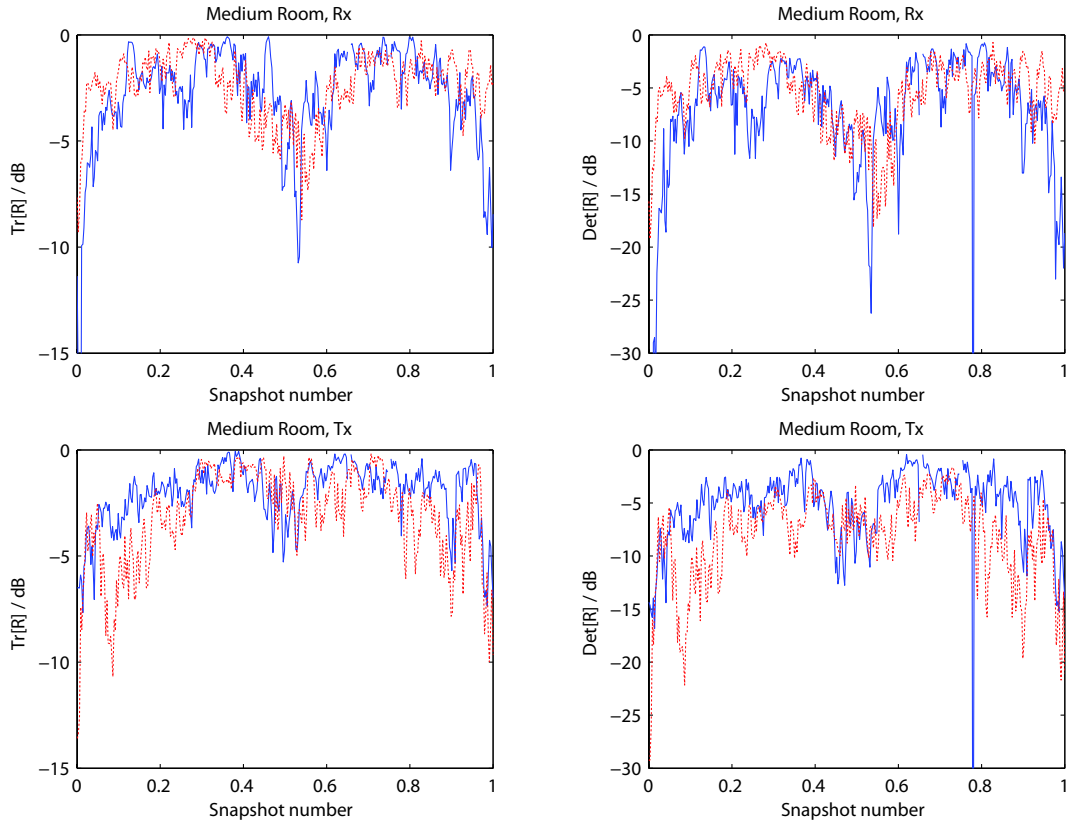


Fig. 7. Trace and determinant of directional spread matrix. Blue solid: 2.55 GHz; red dashed: 5.25 GHz.

environment. In OLoS situations, both mean delay and delay spread are consistently larger at 2.55 GHz.

Figure 6 shows characteristic sample evaluations of strong clustered paths by ISIS in OLoS and LoS situations of the medium-sized laboratory. Clusters appear at identical positions at both frequencies at LoS locations. There are more strong paths, relative to the strongest one, at 5.25 GHz than at 2.55

GHz. Note that this Figure has not been corrected for base-delay (antenna cables, electronics) yet.

V. DIRECTIONAL SPREAD

Recently, a quantification of the 3-D directional spread of a multipath energy distribution has been proposed from an analysis of the second order statistics of small-scale fading

[7]. The second order statistics of the directional energy distribution are contained within the covariance matrix \mathbf{R} :

$$\mathbf{R} = \begin{bmatrix} R_{xx} & R_{xy} & R_{xz} \\ R_{xy} & R_{yy} & R_{yz} \\ R_{xz} & R_{yz} & R_{zz} \end{bmatrix}, \quad (1)$$

where the constituent elements are given by

$$R_{xy} = \frac{1}{2} \sum_{s=1}^{N_s} A_s^2 (d_{x_s} - \bar{d}_x)(d_{y_s} - \bar{d}_y), \quad (2)$$

and

$$\bar{d}_x = \sum_{s=1}^{N_s} A_s^2 d_{x_s} \quad (3)$$

If \mathbf{d}_s denotes the directional unit vector of an outgoing multipath s at the TX or an incoming one at the RX, d_{x_s} is the x-axis component of this s th multipath component, A_s^2 is the power², etc. The trace and the determinant of \mathbf{R} offer useful information about the directional spread of the multipath components³. High $\text{tr}[\mathbf{R}]$ means high RMS directional spread, i.e. multipath components from or to many directions, small $\text{tr}[\mathbf{R}]$ means *limited* directions, i.e. multipath essentially from or to one direction only. The level of variation in second-order statistics of spatial variation with direction is modeled by $\det[\mathbf{R}]$. A low value of $\det[\mathbf{R}]$ means *compact* MPCs, a high value MPCs that are *spread out*. Thus, both $\text{tr}[\mathbf{R}]$ and $\det[\mathbf{R}]$ together determine the distribution of MPCs and how strong the ensuing correlation of the array signals will be.

We calculated $\text{tr}[\mathbf{R}]$ and $\det[\mathbf{R}]$ of the measured incident/outgoing multipath for the RX and TX side and plotted them in log10 scale, normalised to their respective maximum possible values (Figure 7). The calculation was done for the azimuth domain only, so \mathbf{R} reduces to a four-element matrix. Note that we consider only MPC directions that start at the TX and *terminate* at the RX, which is basically the double-directional viewpoint [8]. Still, the analyses at the Rx and the Tx sides we perform here are independent of each other. We do so because we consider directions only, not MIMO coefficients, for which this independence does not generally hold.

The LoS situation at the beginning and the end of the route is evident at both frequencies (compare with route in Figure 2). Also, the OLoS situations bear out as high directional spread and high variation, both at TX and RX. However, at the center of the route, where also LoS existed, the clustering at the Rx is significantly more pronounced than at the Tx.

VI. CONCLUSIONS

From the analysis of the evaluated measurement data, we draw the following conclusions. Surprisingly, power delay profiles (PDPs) at the higher frequency tend to be better delay resolved, despite the same measurement equipment. If

²Note that the total power is normalised to unity, hence $\sum_{s=1}^{N_s} A_s^2 = 1$

³Remember that the trace and the determinant of a matrix are the product and the sum of its eigenvalues, respectively.

present at all, smaller smooth surfaces seem to favour specular reflections, showing up as distinct long-delayed peaks in the PDP. When the environment supports clusters of multipath components, these show up at both frequencies, supporting the clustering approach. There are more significant paths at 5.25 GHz than at 2.55 GHz. The quantification of the directional spread of a multipath energy distribution by second-order statistics of spatial variation of incoming/outgoing waves is a useful metric, because it allows to assess whether relevant multipath comes in clusters or unclustered, separately for TX and RX.

ACKNOWLEDGEMENTS

This work was conducted within the European Network of Excellence for Wireless Communications (NEWCOM). We thank Elektrobit Testing Ltd. for generous support.

REFERENCES

- [1] M. Beach and M. Hunukumbure, "Multi-antenna radio measurements and results," in *Mobile Broadband Multimedia Networks*, L. Correia, Ed. Elsevier, 2006, p. 589.
- [2] B. Maharaj, J. Wallace, L. Linde, and M. Jensen, "Linear dependence of double-directional spatial power spectra at 2.4 and 5.2 GHz from indoor MIMO channel measurements," *IEE Electronics Letters*, vol. 41, pp. 1338–1340, 2005.
- [3] L. Correia, Ed., *Wireless Flexible Personalised Communications (COST 259 Final Report)*. Chichester (UK): Wiley, 2001.
- [4] L. Hentilä, P. Kyösti, J. Ylitalo, X. Zhao, J. Meinilä, and J.-P. Nuutinen, "Experimental characterization of multi-dimensional parameters at 2.45 and 5.25 GHz indoor channels," in *WPMC2005*, Aalborg, Denmark, September 2005, see also <http://www.propsim.com/>.
- [5] B. Fleury, P. Jourdan, and A. Stucki, "High-resolution channel parameter estimation for MIMO applications using the SAGE algorithm," in *2002 International Zurich Seminar on Broadband Communications*, Zurich, Feb. 2002, pp. 30–1 – 30–9.
- [6] A. Richter, "Estimation of radio channel parameters: Models and algorithms," Ph.D. dissertation, Technische Universität Ilmenau, 2005.
- [7] A. Pal, M. Beach, and A. Nix, "A quantification of 3-d directional spread from small-scale fading analysis," *accepted for publication at IEEE International Conference on Communications*, June 2006, Istanbul, Turkey.
- [8] M. Steinbauer, A. Molisch, and E. Bonek, "The double-directional radio channel," *IEEE Antennas and Propagation Magazine*, vol. 43, no. 4, pp. 51 – 63, Aug. 2001.